# Multiscale Impacts of Variable Heating in Climate

PRASHANT D. SARDESHMUKH AND PHILIP SURA

*CIRES Climate Diagnostics Center, University of Colorado, and NOAA/Earth System Research Laboratory, Boulder, Colorado*

(Manuscript received 23 March 2006, in final form 2 April 2007)

ABSTRACT

While it is obvious that the mean diabatic forcing of the atmosphere is crucial for maintaining the mean climate, the importance of diabatic forcing *fluctuations* is less evident in this regard. Such fluctuations do not appear directly in the equations of the mean climate but affect the mean indirectly through their effects on the time-mean transient-eddy fluxes of heat, momentum, and moisture. How large are these effects? What are the effects of tropical phenomena associated with substantial heating variations such as ENSO and the MJO? To what extent do variations of the extratropical surface heat fluxes and precipitation affect the mean climate? What are the effects of the rapid "stochastic" components of the heating fluctuations? Most current climate models misrepresent ENSO and the MJO and ignore stochastic forcing; they therefore also misrepresent their mean effects. To what extent does this contribute to climate model biases and to projections of climate change?

This paper provides an assessment of such impacts by comparing with observations a long simulation of the northern winter climate by a dry adiabatic general circulation model forced only with the observed time-mean diabatic forcing as a constant forcing. Remarkably, despite the total neglect of all forcing variations, the model reproduces most features of the observed circulation variability and the mean climate, with biases similar to those of some state-of-the-art general circulation models. In particular, the spatial structures of the circulation variability are remarkably well reproduced. Their amplitudes, however, are progressively underestimated from the synoptic to the subseasonal to interannual and longer time scales. This underestimation is attributed to the neglect of the variable forcing. The model also excites significant tropical variability from the extratropics on interannual scales, which is overwhelmed in reality by the response to tropical heating variability. It is argued that the results of this study suggest a role for the stochastic, and not only the coherent, components of transient diabatic forcing in the dynamics of climate variability and the mean climate.

## 1. Introduction

Despite significant improvements in climate models over the last two decades, the substantial remaining errors in simulations of both the mean climate and climate variability have proved difficult to eradicate. There is evidently a connection between these two types of error, but attempts at a systematic diagnosis quickly run up against the chicken-or-egg issue of whether the errors in the mean cause those in the variability or vice versa. The elegant theory of adiabatic transient-eddy–mean-flow interactions developed over the last several decades is generally unhelpful in this regard, and it also has limited applicability to finite amplitude variations in zonally asymmetric environments and to diabatically driven flows in the troposphere. Furthermore, there is no reason why GCMs should not be able to handle such adiabatic interactions, other than inadequate model resolution. The fact that many GCM simulation errors are not qualitatively sensitive to further increases of model resolution suggests that the mishandling of such interactions is not the chief culprit. The pointer thus turns toward the misrepresentation of diabatic processes, as manifested in errors of both the mean and transient diabatic heating.

To some extent, a GCM's mean diabatic heating error can be reduced by the (physical or unphysical) tuning of the GCM's parameterizations. Errors in the variable heating are harder to tune away. Many transient atmospheric phenomena associated with strong heating variations continue to be poorly simulated by GCMs. Prime examples are such tropical phenomena as the El

*Corresponding author address:* Prashant Sardeshmukh, CIRES Climate Diagnostics Center, University of Colorado, and NOAA/Earth System Research Laboratory, 325 Broadway, Boulder, CO 80305-3328.
E-mail: prashant.d.sardeshmukh@noaa.gov

DOI: 10.1175/2007JCLI1411.1

Niño–Southern Oscillation (ENSO) and the Madden–Julian oscillation (MJO) that dominate on interannual and intraseasonal time scales. Others are not hard to find. It is also relevant in this context that currently there is almost no explicit accounting in GCMs of the "unparameterized remainder" of feedbacks from the unresolved to the resolved scales at each model time step. Several modeling groups are exploring ways to treat such feedbacks as additional stochastic forcing terms, but without clear guidance as to their potential impact on climate variability and the mean climate.

Our principal aim in this paper is to provide an overall assessment of how diabatic heating variability affects atmospheric circulation variability and the mean climate, and by implication, how improving representations of transient diabatic phenomena and stochastic forcing in climate models would improve simulations of climate variability and the mean climate. We discuss in section 2 how the transient forcing does not affect the mean climate directly but indirectly through its effect on the mean adiabatic transient eddy fluxes, and how its overall effect can be assessed—with some limitations—through model simulations in which it is ignored. To this end, we present in section 3 results from a long 108 000-day perpetual winter simulation by a dry adiabatic general circulation model forced with the observed time-mean diabatic forcing as a constant forcing. The errors of this simulation are attributed to the neglect of the transient forcing. Section 4 addresses potential difficulties with such an attribution. Evidence that the transient forcing has a nonnegligible stochastic component is presented in section 5, and a discussion and concluding remarks follow in section 6.

## 2. Conceptual framework

Consider the atmospheric evolution equations in the form

$$\frac{dx_i}{dt} = L_{ij}x_j + N_{ijk}x_jx_k + F_i, \tag{1}$$

where $x_i$ is the $i$th component of the state vector $\mathbf{x}$, the first and second terms on the right are the linear and quadratically nonlinear adiabatic tendencies (in which we include linear and quadratically nonlinear damping terms), respectively, and all other tendencies are represented by the forcing $F_i$. For convenience we use throughout this paper the Einstein summation convention of summing over repeated indices; thus, $L_{ij}x_j$ actually stands for $\Sigma_j L_{ij}x_j$, etc. Note that $L_{ij}$ and $N_{ijk}$ are constant in time. Now if we write $x_i$ as a sum of mean and transient parts, $x_i = \overline{x}_i + x_i'$, the equation for the mean is

$$\frac{d\overline{x}_i}{dt} = 0 = L_{ij}\overline{x}_j + N_{ijk}\overline{x}_j\overline{x}_k + \underbrace{N_{ijk}\overline{x_j'x_k'}}_{\overline{T}_i} + \overline{F}_i = L_{ij}\overline{x}_j + N_{ijk}\overline{x}_j\overline{x}_k + \overline{T}_i + \overline{F}_i, \tag{2}$$

and the equation for the transients, obtained by subtracting (2) from (1), is

$$\frac{dx_i'}{dt} = \underbrace{(L_{ij} + N_{ijk}\overline{x}_k + N_{ikj}\overline{x}_k)x_j'}_{M_{ij}x_j'} + \underbrace{N_{ijk}x_j'x_k' - N_{ijk}\overline{x_j'x_k'} + F_i'}_{T_i' + F_i'}, \tag{3}$$

where $M$ represents linearization about the mean state and $T'$ the transient adiabatic fluxes. The equation for the eddy covariances $C_{ij} = \overline{x_i'x_j'}$ may then be obtained from (3) as

$$\frac{dC_{ij}}{dt} = 0 = M_{ik}C_{kj} + C_{ik}M_{jk} + \underbrace{[\overline{(T_i' + F_i')x_j'} + \overline{(T_j' + F_j')x_i'}]}_{Q_{ij}}. \tag{4}$$

This equation relates $C$ to the third-order moments $\overline{T'x'}$ and the covariance of $F'$ with $x'$. Note that one can write an equation like (4) in any norm (i.e., for any linear transformation of $x'$). In the energy norm $C_{ij}$ is the energy and $\overline{F_ix_i}$ is the energy source. The impact of the transient forcing $F'$ on the mean climate can thus be seen as occurring through its impact on $C$ (and therefore on $\overline{T}_i$, since $\overline{T}_i = N_{ijk}C_{jk}$) in (4), and then through $\overline{T}_i$ in (2).

Equations (2) and (4) provide a convenient conceptual framework for investigating the interaction between climate variability and the mean climate and how it is affected by the mean and variable diabatic forcing. A significant simplification occurs if the terms $Q_{ij}$ within the square brackets in (4) are expressible in terms of $\overline{x}_i$ and $C_{ij}$ plus external sources; then (2) and (4) form a closed set for $\overline{x}_i$ and $C_{ij}$ and there is no need to explicitly consider (3). One simple way to do this (among others) is to approximate $T_i' + F_i'$ in (3) as stochastic forcing terms $S_{im}\eta_m$, where $\eta_m$ is delta-correlated white noise. The terms within the square brackets in (4) then become $Q_{ij} = S_{im}S_{jm}$, and (2) and (4) reduce to perhaps the simplest possible closed set of coupled equations linking the mean climate and climate variability. Note that in this case, (4) is a linear equation for $C$, and a stationary positive-definite solution exists only if $M$ is a stable linear operator.

Although no one to our knowledge has attempted to solve such a coupled set of equations, much has been learned by analyzing (2) and (4) separately. There is a long history of studies considering simplified forms of (2) to understand the effects of $\overline{F}$ and $\overline{T}$ on the mean

climate $\bar{x}$. A few studies have also used simplified forms of (4) to understand how $C$ is influenced by $\bar{x}$ through $M$. For example, Whitaker and Sardeshmukh (1998, hereafter WS98) solved (4) for the $C$ of the extratropical synoptic eddies, specifying an $M$ corresponding to linearization about the observed long-term mean tropospheric circulation, and also specifying $Q_{ij} = S_{im}S_{jm}$, and obtained remarkably realistic storm tracks. Two aspects of their successful simulation are especially relevant here, as will become evident in the following pages: 1) their model was sufficiently damped so that $M$ was stable, as required; and 2) in order to obtain realistic storm-track magnitudes over the entire Northern Hemisphere, they adjusted the overall magnitude of their $Q_{ij}$ terms by a single global factor. Thus their success was partly due to their implicitly accounting for the contribution of the $F'$ terms in (4), albeit in a crude manner.

We are concerned in this paper with the effect of $F'$ not just on $C$ but also on the mean $\bar{x}$, and a consistent treatment requires that we consider (2) and (4) together. We recognize that while the $Q_{ij} = S_{im}S_{jm}$ approximation is illuminating, it may not be accurate enough for a quantitatively useful diagnosis of a GCM's erroneous simulated mean and variability. Such a closure of $Q$, or indeed any closure at all, is in fact unnecessary in (4) if we consider (3) explicitly [i.e., if we run the model (1) with prescribed mean and variable forcings]. To generate the long simulation described in the next section, we forced a dry adiabatic GCM with only the mean observed forcing and interpreted the errors in its simulated mean and variability as arising from the neglect of the variable forcing $F'$. Despite some potential difficulties with this interpretation discussed later in the paper, we are confident that the errors of our constant-forcing simulation do provide useful estimates of the net impacts of diabatic heating variability on atmospheric circulation variability and the mean climate.

## 3. A constant-forcing simulation

To assess the net impacts of the diabatic forcing variability, we performed a long 108 000-day perpetual winter integration of a dry adiabatic GCM forced with only the observed winter-mean diabatic forcing as a constant forcing. For this purpose we used a T42 5-level version of the University of Hamburg's Portable University Model of the Atmosphere (PUMA), which may be downloaded (see http://www.mi.uni-hamburg.de/Theoretische_Meteorologie.6.0.html). The model has been used in several studies of extratropical storm-track dynamics and climate variability (Fraedrich et al. 2005a,b,c). It incorporates simple parameterizations of thermal and mechanical damping similar to those used by Hoskins and Simmons (1975) and Hall (2000). Specifically, a horizontal $\nabla^8$ hyperdiffusion with a time scale of 6 h at the smallest resolved scale is included in the equations for vorticity, divergence, and temperature. An additional scale-independent but level-dependent linear damping is also imposed on these variables. For vorticity and divergence this linear damping is strongest (1 day) at the lowest model level ($\sigma = 0.9$) and much weaker (30 days) at higher levels. Similarly for temperature, the linear damping is strongest at the lower levels (1 day at $\sigma = 0.9$ and 5 days at $\sigma = 0.7$) and much weaker (30 days) at higher levels. The time-integration scheme is a filtered leapfrog scheme (Asselin 1972) with a time step of 30 min and the filter parameter set to 0.02.

We estimated the observed mean $\overline{F}$ as the (sign reversed) average initial tendency of the *unforced* adiabatic model (1) initialized by the daily averaged 6-hourly wintertime National Centers for Environmental Prediction–National Center for Atmospheric Research (NCEP–NCAR) observational reanalyses of 1970–99, plus the small long-term observed tendency associated with the 30-yr trend. [The NCEP dataset used was actually a "chi-corrected" version generated by modifying the 6-hourly wind divergence fields to balance the large-scale vorticity and mass budgets (Sardeshmukh 1993; Sardeshmukh et al. 1999). The particular advantage of using such a corrected dataset is that there are no spurious vorticity or mass sources in the diagnosed $F$ arising from data analysis errors in the horizontal wind divergence fields.] A similar procedure was followed by Hall (2000) with a T21 5-level model like ours, and by Lin and Derome (1996), Marshall and Molteni (1993), and Roads (1987) with T21 3-level and 2-level quasigeostrophic models. All of these investigators used much shorter observational records to estimate $\overline{F}$. All, like us here, then integrated their models with $\overline{F}$ but for different purposes and for much shorter periods than our 108 000-day run. The study of Hall (2000) was closest to ours, and our results are generally consistent with his results.

In this section, we present some basic comparisons of our constant-forcing simulation with observations to provide a flavor of its realism and deficiencies. We begin with hemispheric one-point correlation maps (also known as one-point teleconnection maps; see Wallace and Gutzler 1981) with respect to base points in the North Pacific and North Atlantic regions of strongest observed synoptic and low-frequency variability, follow up with hemispheric maps of geopotential height variance and momentum and heat fluxes, then with latitude–height cross sections of the zonal means of these quan-

tities, and end with a comparison of the simulated and observed mean climates.

### *a. One-point correlation maps of 500-mb height variability*

To facilitate comparisons of the simulated and observed variability on different time scales, we filtered the 500-mb-height daily time series at each grid point using a 21-point Lanczos filter (Duchon 1979) to isolate variations with periods between 2 and 6 days (the "synoptic" band), greater than 10 days (the "low-frequency" band), between 10 and 90 days (the "intraseasonal" band), and greater than 180 days (the "interannual" band). As a further check on the robustness of some of our surprising interannual band results, we also compared the variability of the simulated 90-day averages with that of observed 90-day averages.

Figure 1 compares the simulated and observed simultaneous and ±2 day lag correlations of 500-mb height variations in the synoptic band for base points in the North Pacific and North Atlantic regions of strongest observed synoptic variability. Note that to enable a cleaner comparison of the simulated and observed correlations in these and all other such maps to follow, the base points in the simulation plots were chosen to be identical to those in the observational plots. These base points may be identified on the zero-lag correlation plots as the points at which the correlation is unity. To save space, Fig. 1 also combines the two separate correlation patterns obtained for the Pacific and Atlantic base points into a single map, as the geographical overlap of the separate patterns is negligible.

Given the vast simplicity of our model vis-à-vis state-of-the-art GCMs, plus the neglect of *all* variable forcing, the general agreement of the simulated and observed synoptic-eddy correlations in Fig. 1 must be regarded as remarkable. Consistent with numerous previous studies, this confirms that to a first approximation the dynamics of extratropical synoptic variability are adiabatic. Closer comparison of the simulated and observed panels, however, reveals significant local discrepancies, such as a tendency for the eddies to propagate too strongly southeastward at the eastern end of the Pacific storm track, and to split into poleward and equatorward propagating eddies at the eastern end of the Atlantic storm track. To what extent such discrepancies are primarily due to model deficiencies or the neglect of the transient forcing is unclear at present. It is also interesting that the statistically significant impact of ENSO on winter-mean storm tracks documented by Sardeshmukh et al. (2000), Compo et al. (2001), Compo and Sardeshmukh (2004), and others, which contributes to the observed but not the simulated panels in Fig. 1, is minor in terms of this statistic. From the equatorward (poleward) shift of the eastern half of the Pacific storm track during El Niño (La Niña), one would expect the observational correlation contours to be more meridionally elongated and bow shaped than the model contours in the eastern Pacific, but the effect is very slight.

Figure 2 shows the observed and simulated 1-point correlations of the low-frequency (>10 day) 500-mb height variations with those at base points in the North Atlantic (top panels) and North Pacific (bottom panels) basins. For the North Atlantic base point, the agreement between the simulated and observed correlations is almost as good as in Fig. 1, but for the North Pacific base point it is not. The simplest interpretation of this is that the neglected transient forcing has a relatively large impact in the Tropics and the Pacific–North American (PNA) sector but not in the region of the North Atlantic Oscillation (NAO). The former is not surprising given our neglect of all tropical diabatic forcing variations associated with the MJO and ENSO that have large impacts in the Tropics and the PNA sector. The relatively minor impact of the transient forcing on the spatial structure of NAO variability is, however, a surprise with implications for the magnitude of the effect of North Atlantic as well as tropical SST variations on the NAO.

To clarify the impacts of transient forcing on the spatial structures of intraseasonal (10–90 day) and lower frequency (>180 day) circulation variability, Figs. 3 and 4 present the 1-point correlations on these time scales in an identical format to that of Fig. 2. (Note again that the base points in these and all such figures in this paper were chosen to correspond to those with the largest observed variability in the Pacific and Atlantic basins in their respective frequency bands.) In Fig. 3, the simulated intraseasonal correlations again match well with those observed in the Atlantic sector. More surprisingly, they also match much better in the Pacific sector than in Fig. 2, the main difference being that the simulated lobe of negative correlations upstream of the base point is shifted farther west into China compared to its position over Kamchatka in the observations. If we attribute this difference to the neglect of MJO heating, then the lower panels of Fig. 3 suggest that the MJO significantly affects the spatial structure of subseasonal variability over East Asia and the northwest Pacific.

Figure 4 presents the 1-point correlations of the interannual and longer-term 500-mb height variations with periods greater than 180 days. The simulated and observed correlation patterns are again very similar for the North Atlantic base point. For the Pacific base point, they are also similar in the mid- and high latitudes, but radically different—even in sign—in the

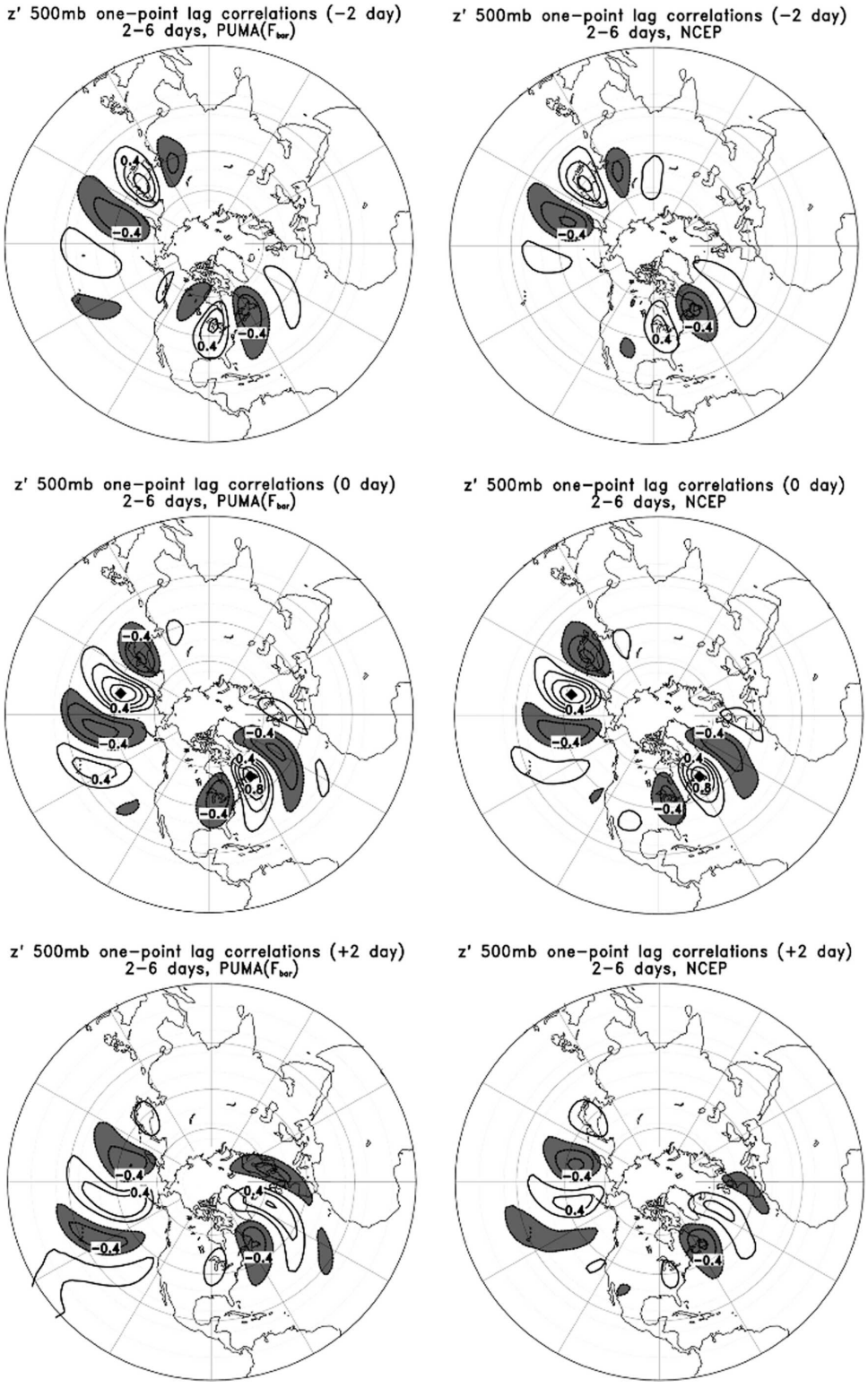


FIG. 1. Time-lag correlations of 500-mb geopotential height fluctuations in the synoptic (2–6-day period) band with those at base points in the northwest Pacific and northwest Atlantic basins in the (left) constant forcing simulation and (right) observations. The contour interval (CI) is 0.2 and values less than −0.2 are shaded. The zero contour is suppressed.

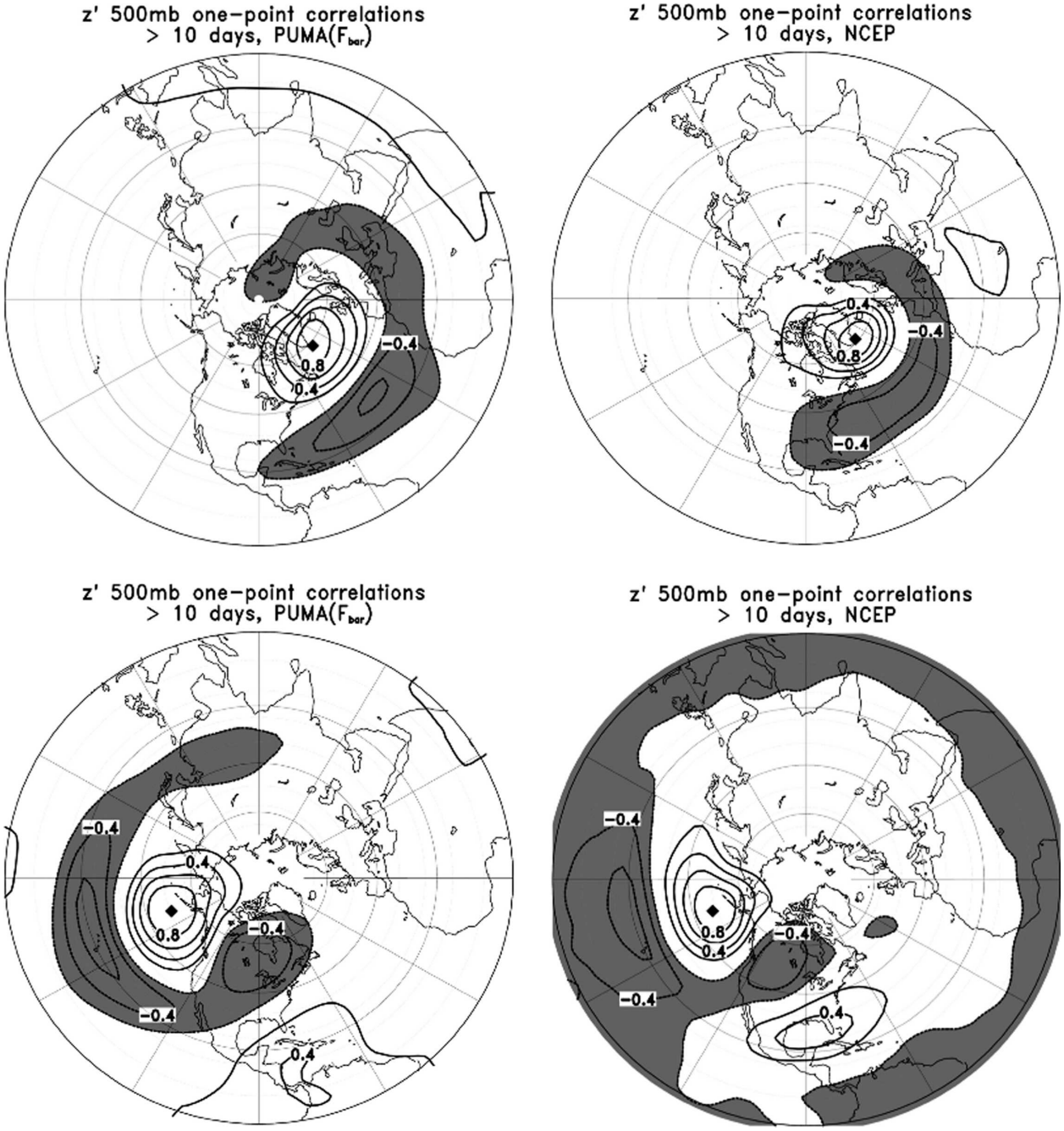


FIG. 2. Correlations of low-frequency 500-mb height variations (with periods greater than 10 days) with those at a reference base point in the (top) North Atlantic and (bottom) North Pacific in the (left) constant-forcing simulation and (right) observations. Contouring as in Fig. 1.

Tropics and subtropics. The observed negative tropical correlations are consistent with ENSO variability, but the simulated correlations—without ENSO variability—are also equally large throughout the Tropics, and *positive*. This is a major surprise. To confirm that the discrepancy is not somehow an artifact of our frequency filter, Fig. 5 shows, in an identical format to Fig. 4, the 1-point correlation maps for 90-day-average 500-mb height variations with respect to the North Pacific base point. The result is very similar to that in the lower panels of Fig. 4. The simulated correlation maps for the height variations at other vertical levels (not shown) are also similar. The positive tropical correlations are in fact strongest ($>0.6$) at 300 mb and decrease above and

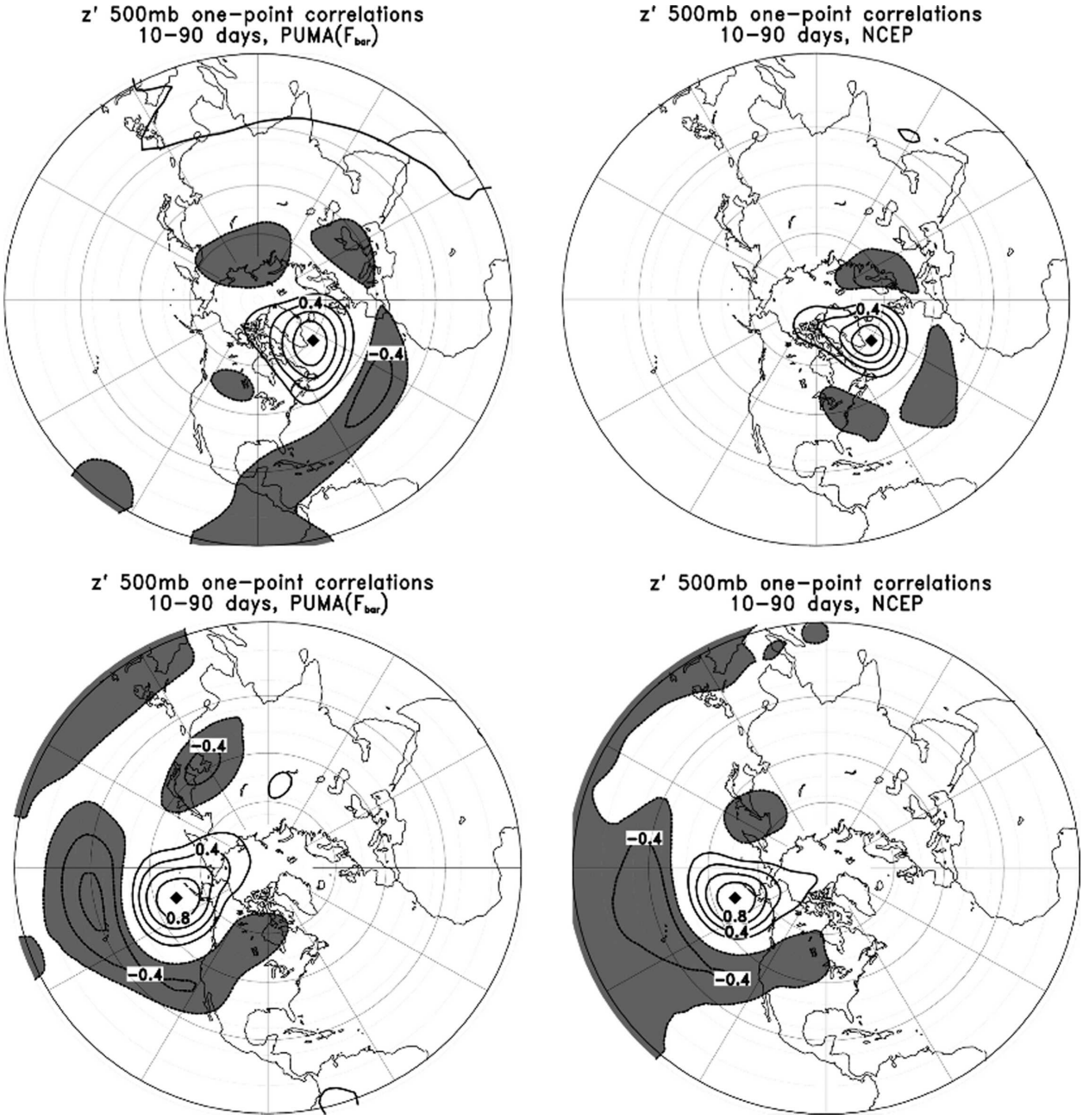


FIG. 3. As in Fig. 2 but for 500-mb geopotential height variations in the intraseasonal frequency band (with periods between 10 and 90 days).

below that level; they are nearly zero at 700 mb and slightly negative at 900 mb.

Since there is no transient forcing in our model, there is no mechanism to generate tropical variability except by extratropical excitation. Consistent with this, Fig. 6 shows that the running 90-day averages of tropically averaged (20°N–20°S) 500-mb heights lag the running 90-day averages of 500-mb heights at the North Pacific base point by about 10 days. The smaller tropical correlations from 300 mb downward are also consistent with excitation from the jet level in midlatitudes.

In summary, Figs. 1–4 contain two surprises. The first is the suggestion that transient diabatic forcing has only a minor impact on the spatial structures of Northern Hemispheric circulation variability. The second is that on interannual and longer scales, extratropical variability can excite significant spatially coherent geopotential height variability in the Tropics.

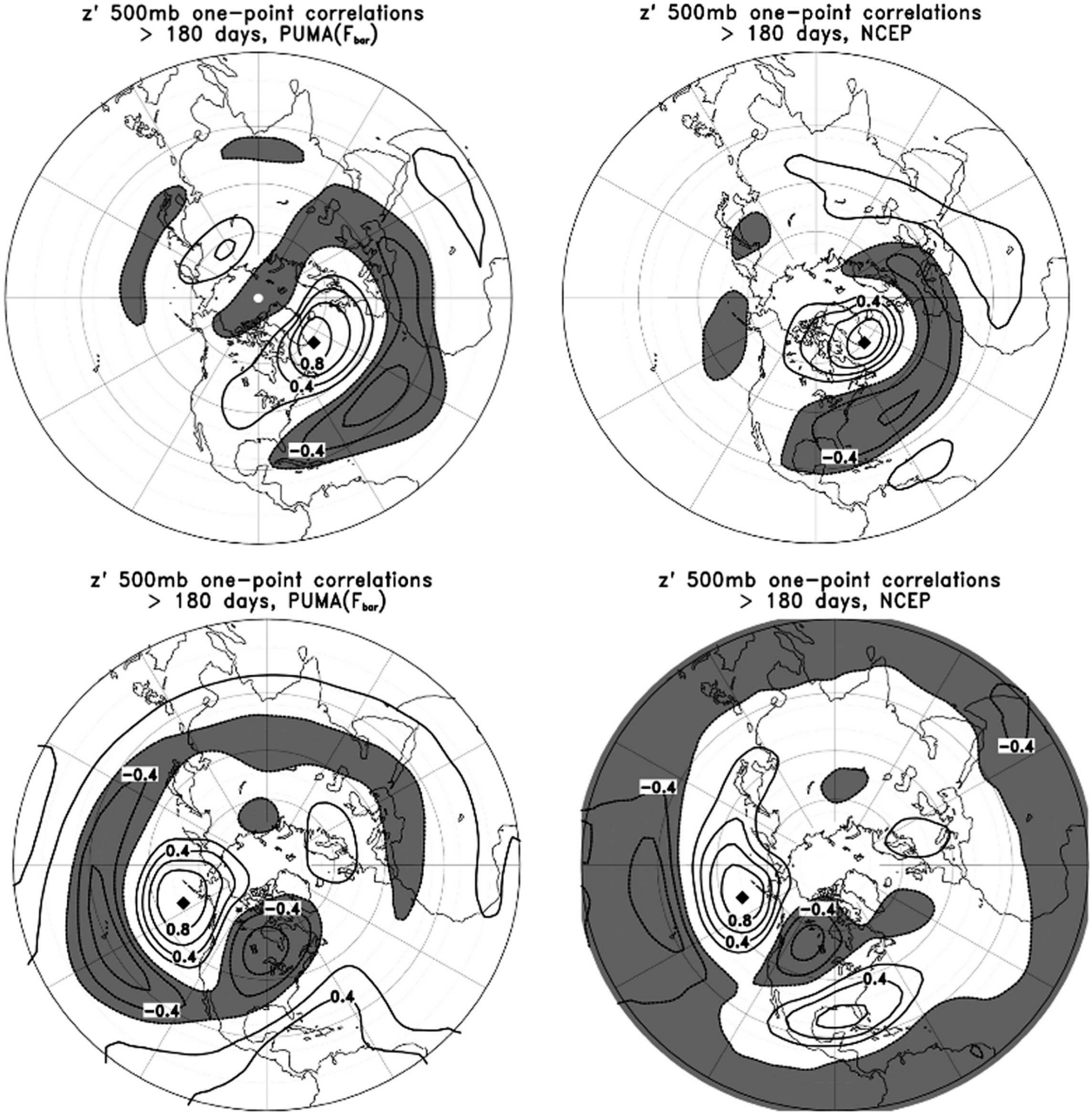


FIG. 4. As in Fig. 2 but for interannual and longer-term 500-mb height variations (with periods greater than 180 days).

We hasten to add that while the effects of the transient forcing on the *spatial structures* of extratropical circulation variability are minor, the effects on their *magnitudes* are not. Table 1 summarizes the standard deviations of the observed and simulated 500-mb height variations in the different frequency bands, at our selected North Atlantic and North Pacific base points as well as averaged over the hemisphere poleward of 20°N. The magnitude of the variability is consistently underestimated in our constant forcing simulation, with the underestimate being relatively minor (10% or less) on the synoptic scale and worsening to as much as 50% on interannual and longer scales.

### *b. Hemispheric maps of variances and fluxes*

Figure 7 compares three different aspects of the simulated daily variability with observations: the mean transient-eddy poleward zonal momentum flux in the upper troposphere (top panels), the mean transient-

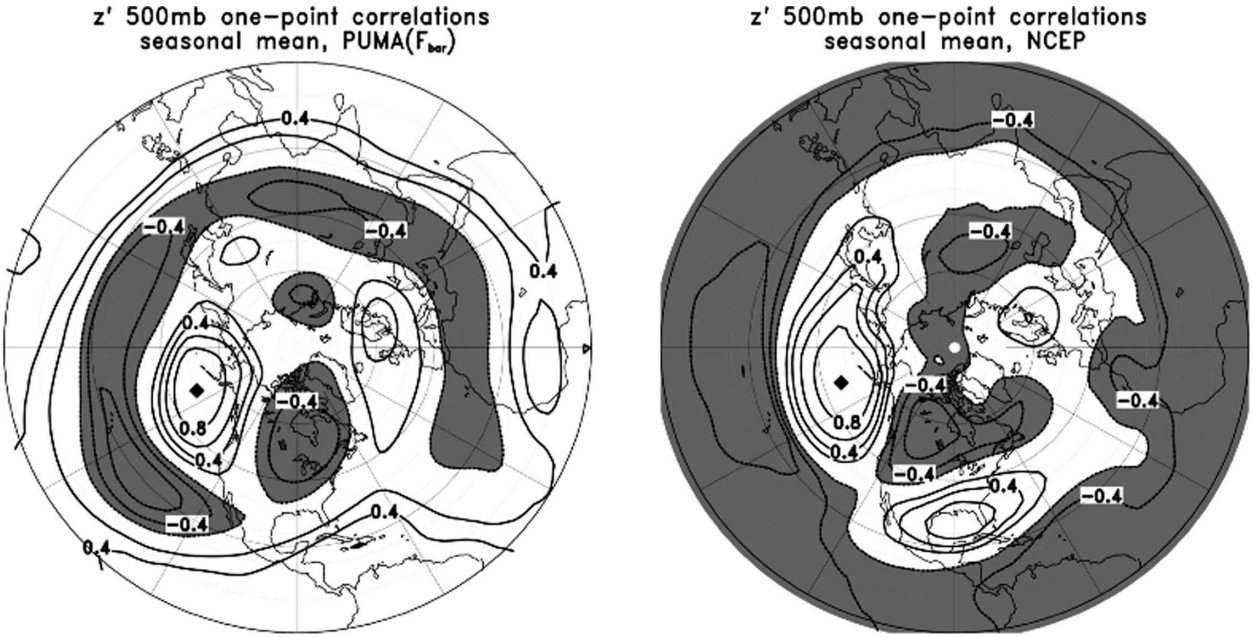


FIG. 5. As in Fig. 4 but for 90-day-average 500-mb height variations.

eddy poleward temperature flux in the lower troposphere (middle panels), and the standard deviation of daily 500-mb heights (bottom panels). Consistent with the results of the previous subsection, the geographical distributions of all three quantities are reasonably well simulated, but their magnitudes are underestimated. The momentum fluxes are somewhat stronger than observed (except over North Africa), whereas the heat fluxes and height variability are clearly weaker.

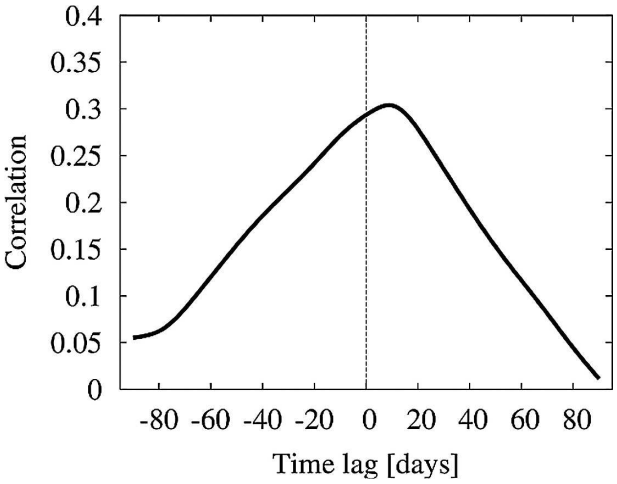


FIG. 6. Simulated time-lag correlation of running 90-day average of tropically averaged (20°N–20°S) 500-mb height variations with running 90-day average 500-mb height variations at the North Pacific reference base point used in Fig. 5. Positive lag corresponds to the tropical heights lagging the North Pacific heights.

### c. Zonal mean fluxes and variability

Figure 8 shows that the meridional and vertical variations of the zonally averaged poleward fluxes of zonal momentum and temperature, as well as the zonally av-

TABLE 1. Rms of filtered 500-mb geopotential height variations in the indicated frequency bands averaged over (top) the hemisphere poleward of 20°N and at selected points in the (middle) North Atlantic and (bottom) North Pacific. The observed and simulated values are listed under the "NCEP" and "PUMA (F_bar)" headings, respectively. Units are in meters.

| Averaged over the northern extratropics (lat: 20°–90°N, lon: 0°–360°) | | |
|---|---|---|
| | NCEP | PUMA (F_bar) |
| 2–6 days | 26.10 | 25.54 |
| 10–90 days | 38.61 | 31.15 |
| >180 days | 63.17 | 41.32 |
| >10 days | 84.01 | 59.18 |
| At North Atlantic base points | | |
| | NCEP | PUMA (F_bar) |
| 2–6 days | 62.70 | 61.18 |
| 10–90 days | 67.20 | 43.91 |
| >180 days | 113.50 | 56.61 |
| >10 days | 148.66 | 82.06 |
| At North Pacific base points | | |
| | NCEP | PUMA (F_bar) |
| 2–6 days | 49.63 | 44.22 |
| 10–90 days | 64.23 | 42.05 |
| >180 days | 116.13 | 66.87 |
| >10 days | 150.40 | 90.25 |

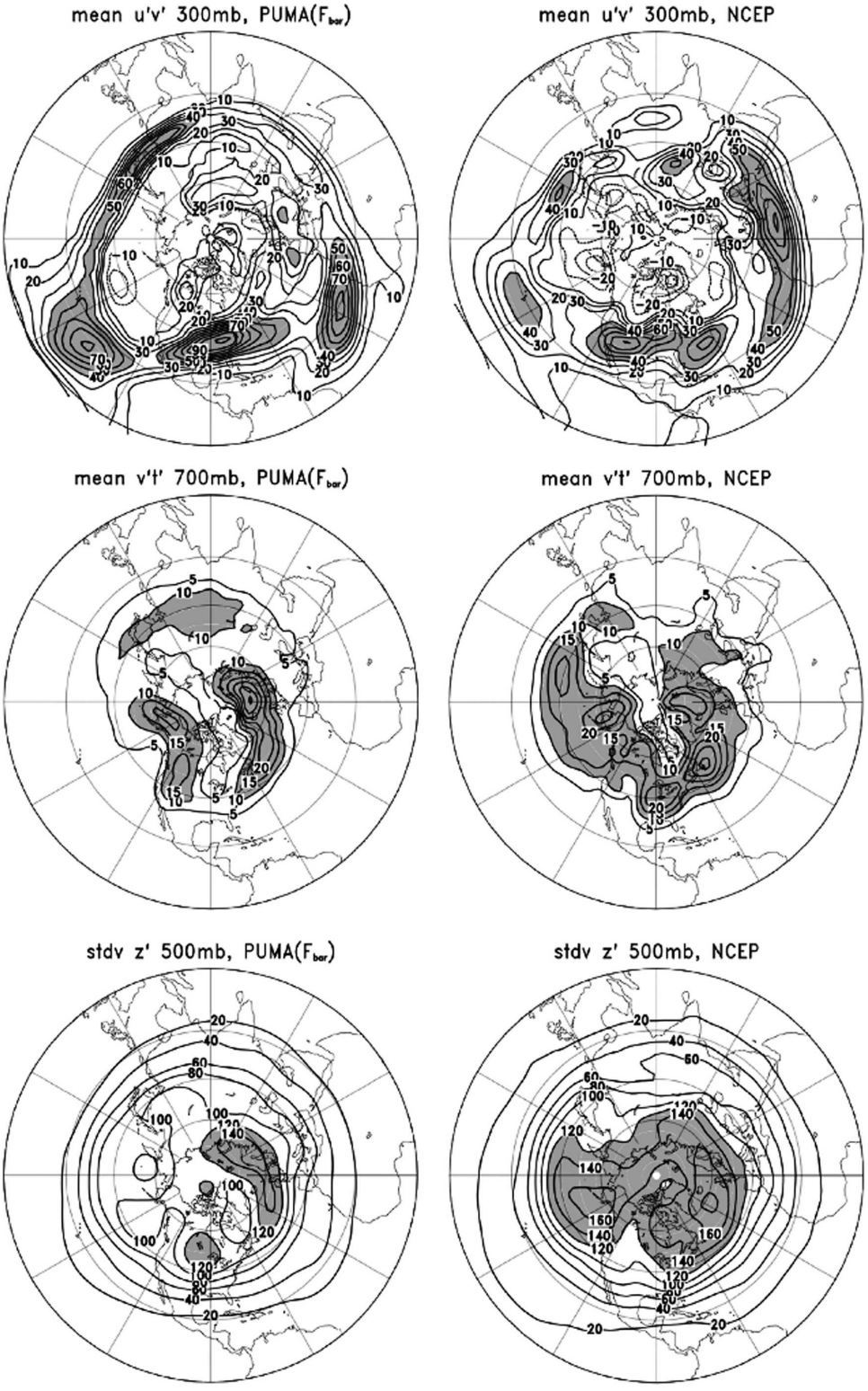


FIG. 7. (left) Simulated and (right) observed statistics of daily variability. (top) Mean poleward zonal momentum flux ($m^2\ s^{-2}$) at 300 mb. (middle) Mean poleward heat flux ($K\ m\ s^{-1}$) at 700 mb. (bottom) Std dev of 500-mb heights (m). Negative values are dashed. Large positive values are shaded for clarity.

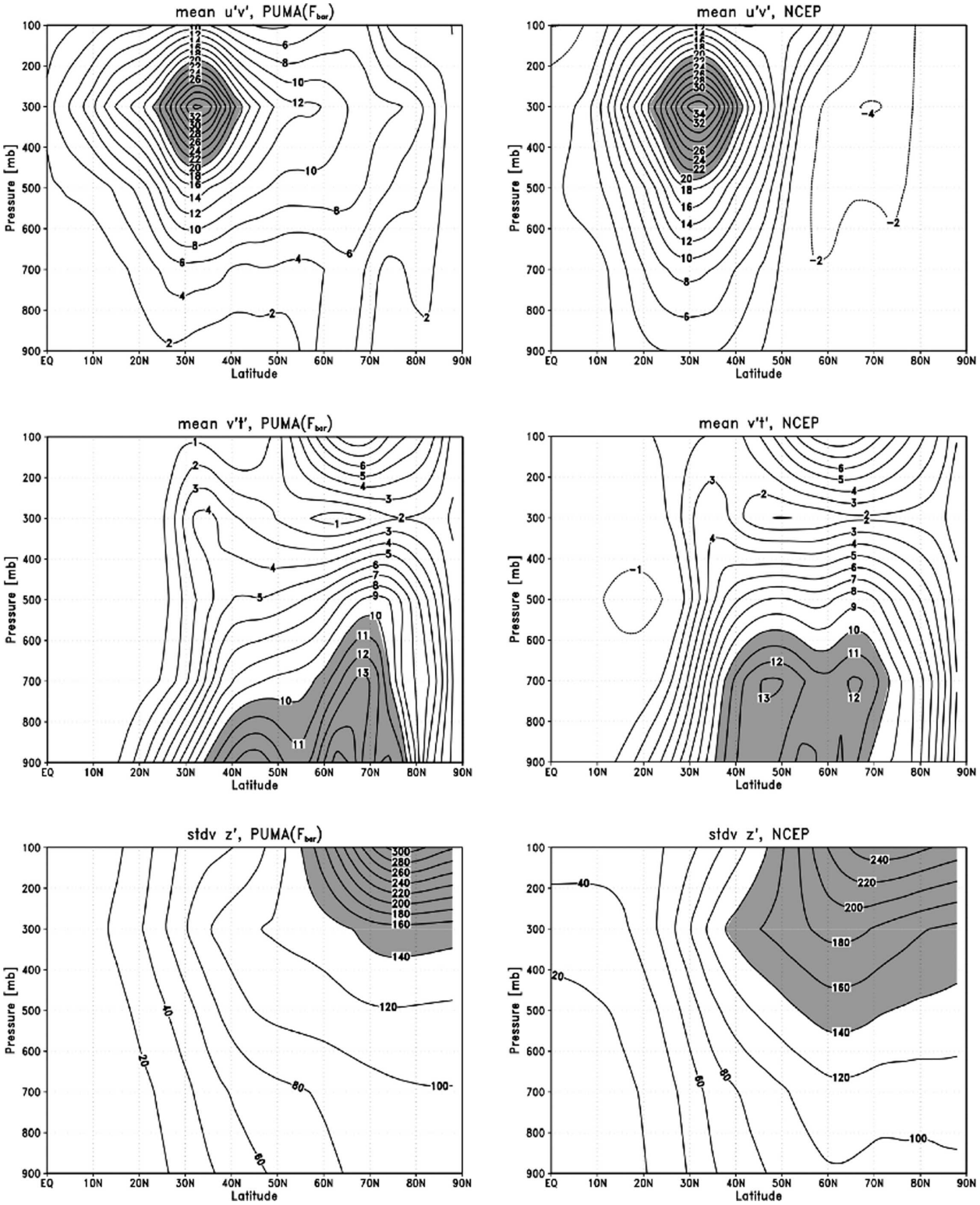


FIG. 8. As in Fig. 7 but for the latitude and height variation of the zonally averaged (top) poleward momentum flux, (middle) poleward heat flux, and (bottom) std dev of geopotential heights of the (left) simulated and (right) observed daily variability. Large positive values are shaded for clarity. Negative values are dashed. The zero contour is not shown.

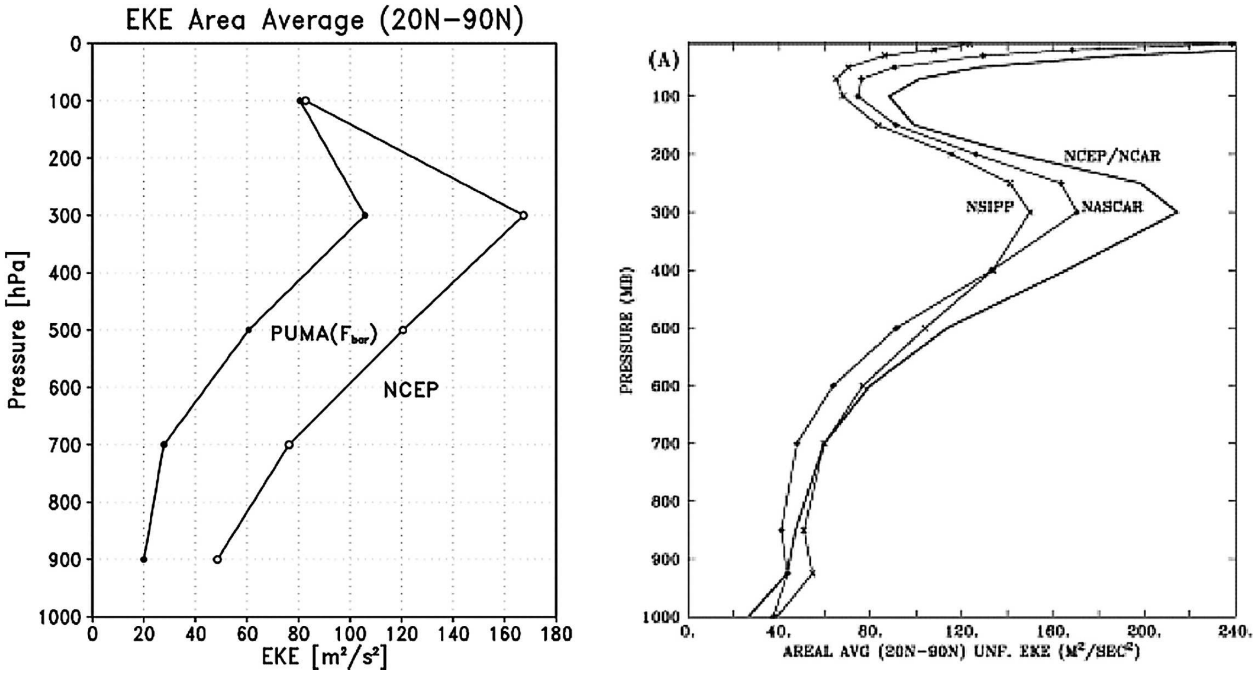


FIG. 9. (left) Vertical profiles of simulated and observed EKE averaged over the northern extratropics (20°–90°N). (right) A similar plot adapted from Robinson and Black (2005) of the observed EKE for 1979–96 and for two NASA GCM simulations of that period with prescribed observed SSTs.

eraged standard deviations of geopotential heights, are also well simulated. The principal deficiencies are a generally weaker height variability than observed, except in the polar stratosphere where it is stronger; weaker lower-tropospheric temperature fluxes above the boundary layer in midlatitudes; and momentum fluxes of the wrong sign in high latitudes.

From Eq. (4), one expects the neglect of transient forcing to lead to an overall reduction of eddy kinetic energy (EKE). The left panel of Fig. 9 compares the vertical profiles of the simulated and observed transient eddy kinetic energy averaged over the hemisphere poleward of 20°N. Consistent with the lower panels of Figs. 7 and 8, the simulated EKE is indeed significantly weaker than observed. It is interesting that a similar error also occurs in the state-of-the-art National Aeronautics and Space Administration (NASA) GCMs with much higher vertical resolution, documented by Robinson and Black (2005) and reproduced here in the right panel of Fig. 9. One wonders to what extent it is also due to weak transient diabatic forcing in those GCMs.

### *d. Time-mean maps*

Finally, Fig. 10 compares the simulated and observed long-term fields of 500-mb heights and mean sea level pressure. The observational averages are over the same 30 winters used for calculating $\overline{F}$; the model averages are over the 108 000 simulated days. The agreement is generally reasonable, except that at both levels the model's pressure ridge over western Canada and the pressure low over the Pole are too strong. The model's 500-mb height biases over Canada are brought into sharper focus in the comparison in Fig. 11 of the zonally asymmetric portions of the simulated and observed height fields. These biases are certainly not small, but given our neglect of *all* transient diabatic forcing and the model's obvious deficiencies (especially its crude vertical resolution), it would be surprising if they were much smaller. Nonetheless, it is noteworthy that a similar error over western Canada, and of a similar magnitude, occurs in a 34-level NASA Seasonal-to-Interannual Prediction Project (NSIPP) GCM simulation with prescribed observed SSTs for 1979–96 (Robinson and Black 2005; see their Fig. 1). It is also interesting to compare our upper-tropospheric stationary wave biases with those of the Geophysical Fluid Dynamics Laboratory Atmosphere Model version 2.0 (GFDL AM2; Anderson et al. 2004) and NCAR/Community Atmosphere Model version 3 (CAM3; Hurrell et al. 2006) atmospheric GCMs.

We have visually compared these and many other aspects of our simulation with those of other GCMs in the published literature. Our mean biases are generally within the range of biases of GCMs participating in the

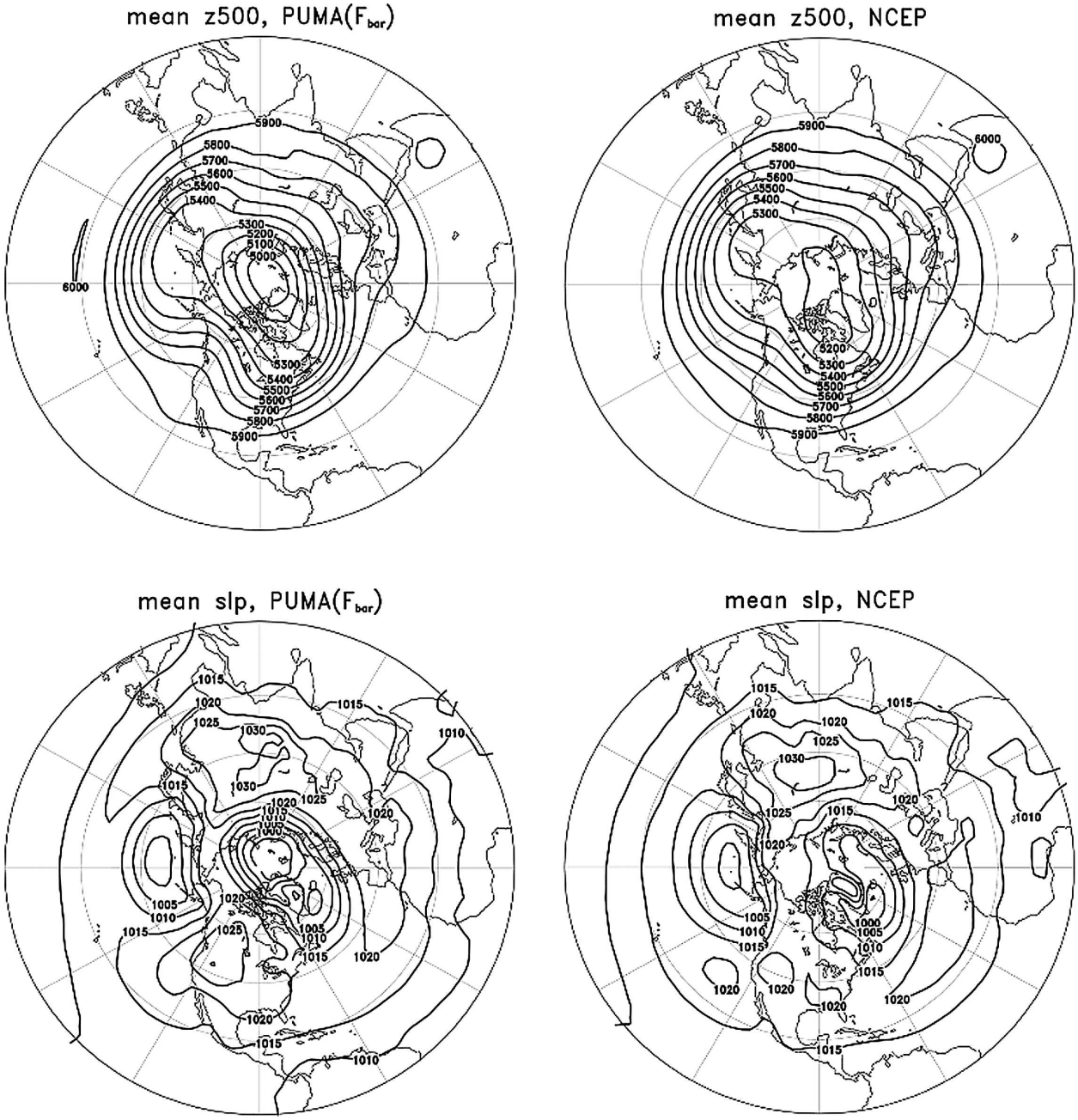


FIG. 10. The wintertime [December–February (DJF)] long-term mean field of (top) 500-mb geopotential heights and (bottom) mean sea level pressure in the (left) constant forcing simulation and in the (right) NCEP–NCAR reanalyses. The CI is 100 m for the 500-mb heights and 5 hPa for the sea level pressure.

Atmospheric Model Intercomparison Project (AMIP; Gates et al. 1999). For various reasons, documentations of even basic measures of GCM-simulated circulation variability such as shown here are not as yet widely available, possibly because regular archival of the voluminous daily output from long GCM runs is a relatively recent practice. It would certainly be interesting to assess to what extent, if any, the current generation of atmospheric and coupled GCMs are better at reproducing the aspects of observed extratropical circulation variability depicted in Figs. 1–8 than our simple model with specified observed time-mean forcing.

## 4. Attribution to transient forcing

To what extent can the deficiencies of our constant-forcing simulation be attributed solely to our neglect of

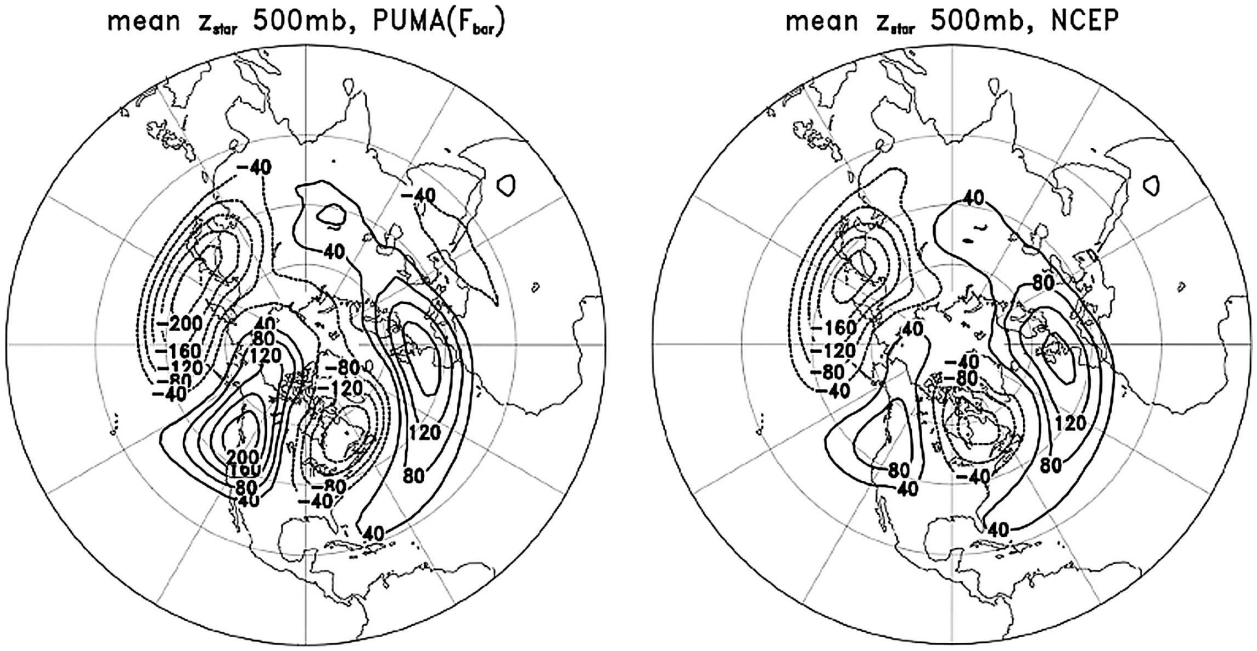


FIG. 11. As in Fig. 10 but for the (left) simulated and (right) observed long-term mean zonally asymmetric 500-mb geopotential height fields. The CI is 40 m, and negative values are dashed. The zero contour is not shown.

$F'$? There can be little doubt that the model's limited T42 5-level resolution and the errors in its simple damping parameterizations also contribute. Is it possible that our relatively weak simulated variability is due to excessive damping? The fact that the NASA models also show a similar weakness in Fig. 9 is reassuring in this regard, but not conclusive, since the damping could be excessive in those (and other) GCMs as well.

Clearly, our model is not so strongly damped that it has no variability; the issue is just whether the damping is stronger than in reality. We do not believe this to be case after performing the following additional simulation with a constant forcing $\overline{F}_{ci} = \overline{F}_i + \overline{T}_{oi}$, where $\overline{T}_{oi}$ is the observed mean transient-eddy flux. This forcing is simply the sign-reversed initial tendency of the unforced model (1) when initialized with the observed mean climatology, plus the small tendency of the 30-yr trend. In an excessively damped model, such a forcing would maintain a constant model state (i.e., the observed mean state), and there would be no variability. In other words, the linear operator $M$ in (3) would be stable, and (4) would have a trivial null solution. The issue thus boils down to whether the observed mean state is stable or unstable for realistic damping. Hall and Sardeshmukh (1998) examined this matter in some detail and concluded that the observed mean state was close enough to being neutral that it was "pointless to come down on one side of the fence or the other." As mentioned earlier, WS98 simulated realistic storm tracks using damping parameters that rendered $M$ weakly stable. These studies, as well as theories of baroclinic adjustment, suggest that for realistic damping $M$ is neutral or weakly stable. By this logic, we should obtain little or no variability in our $\overline{F}_c$ run if our damping is realistic.

As Fig. 12 shows, the variability is indeed considerably weaker in this run than in the $\overline{F}$ run, but is not zero, which suggests that if anything, our damping may be too *weak*, not too strong. We therefore conclude that despite our model's limitations, our results do indicate a substantial role for diabatic forcing variations in influencing not only climate variability but also the mean climate.

Another potential concern with our diagnosis is the decoupling of the forcing and the circulation (i.e., the specification of diabatic heating as an "external" forcing). Similar concerns also arise when diagnosing any subsystem of the complete coupled climate system with a subsystem model and representing all other influences as external or boundary forcing. This is not a black-or-white issue but one with varying shades of gray, depending on the problem at hand. For example, despite the obvious coupling of the atmosphere and the ocean, a great deal has been learned about their dynamics and variability using atmospheric and oceanic GCMs with prescribed SST and surface wind stress and heat flux "forcings," respectively. The decoupling issue becomes relatively more important when a mechanical

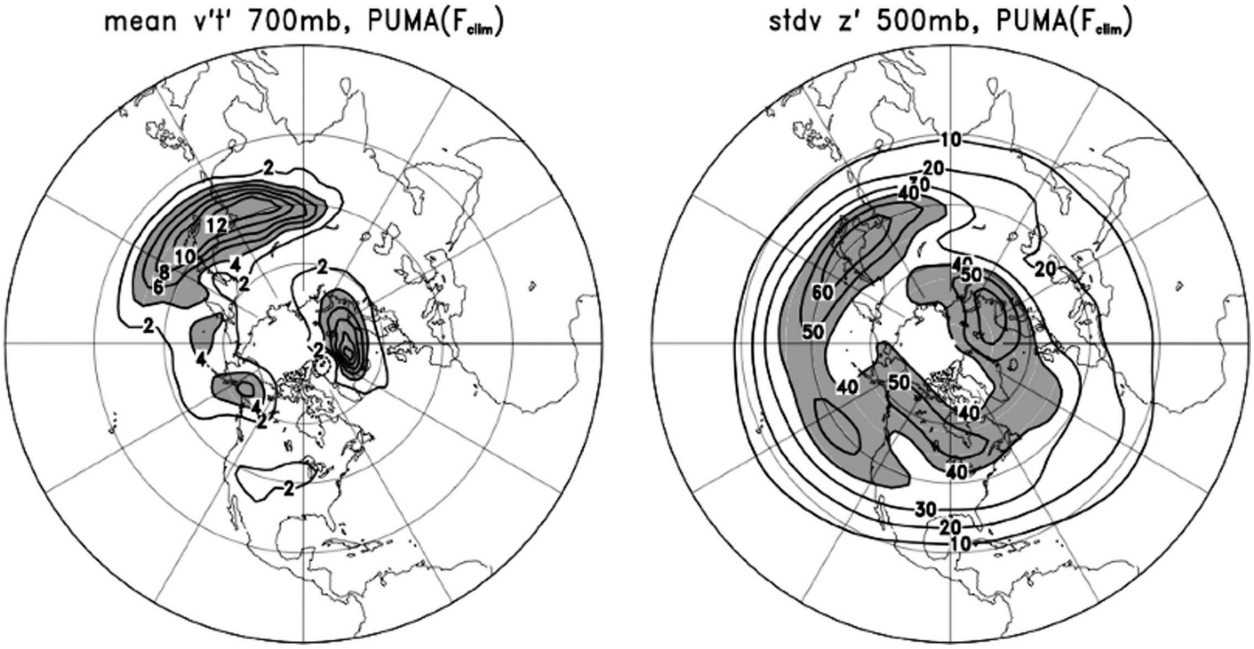


FIG. 12. Simulated (left) 700-mb poleward transient-eddy heat flux (K m $s^{-1}$) and (right) std dev of daily 500-mb heights (m) in a constant forcing simulation in which the forcing is the sum of the mean diabatic forcing and forcing by the mean adiabatic transient-eddy fluxes. These panels should be compared with their counterparts in Fig. 7. Note the smaller CIs and smaller values here.

or thermal damping mechanism is mis-specified as a forcing $F'$; this can alter the sign of $\overline{F'x'}$ in (4) and introduce spurious energy sources and sinks in the system. We do not believe the forcing-circulation decoupling to be a serious concern here partly because we do not have $F'$ in our constant-forcing simulation, so the question of whether or not it is strongly coupled to the system state is largely irrelevant. The underestimation of the eddy kinetic energy in Fig. 9 also clearly suggests the need for an additional energy source, that is, a forcing, not an energy sink.

## 5. Evidence of stochastic transient forcing

Our realistic simulations of the synoptic and intraseasonal correlation structures in Figs. 1 and 3, considered together with the success of stochastically driven damped linear models of extratropical variability on these time scales (Farrell and Ioannou 1995; WS98; Winkler et al. 2001; Newman et al. 2003; Delsole 2004; Newman and Sardeshmukh 2008), suggest that a portion of the transient adiabatic nonlinear and diabatic forcing terms [$T' + F'$ in Eq. (3)] may be treated as a modified linear dissipation plus stochastic forcing. We consider this evidence below and then provide additional observational evidence that outside the Tropics, $F'$ has a nonnegligible stochastic component.

WS98 obtained realistic synoptic correlation patterns in a stochastically forced damped linear model (see their Figs. 6 and 7) and also realistic amplitudes by adjusting the amplitude of their stochastic forcing with a single global constant. The fact that we too obtained realistic patterns (Fig. 1) in a nonlinear model without transient diabatic forcing, and with only slightly reduced amplitudes (Table 1), suggests that diabatic transients [$F'$ in (3)] play a relatively minor role in the dynamics of synoptic variability, except at the eastern ends of the Pacific and Atlantic storm tracks as mentioned earlier. It also suggests that (3) may be approximated as follows:

$$\begin{aligned}\frac{dx_i'}{dt} &= M_{ij}x_j' + \underbrace{\qquad T_i' \qquad} + \underbrace{\qquad F_i' \qquad} \\ &\simeq M_{ij}x_j' + (D_{ij}x_j' + S_{1ip}\eta_p) + (E_{ij}x_j' + S_{2iq}\eta_q) \\ &\simeq \tilde{M}_{ij}x_j' + S_{im}\eta_m, \end{aligned} \tag{5}$$

in which $T'$ and $F'$ are first approximated as linear terms in $x'$ plus noise, and then all the linear deterministic and stochastic dynamics are collected in the linear operators $\tilde{M}$ and $S$. WS98 explicitly considered a model of this form, accounting for their neglect of $T'$ and $F'$ by approximating, in effect, the operator $D + E$ as a simple damping $-\alpha I$ and explicitly specifying a stochastic forcing $S = S_1 + S_2$ as uncorrelated white noise with covariance $Q = SS^T \sim cI$. The realism of their results

despite these drastic simplifications was striking, and supports the gross validity of (5). In our nonlinear constant-forcing simulations, we explicitly modeled $T'$ but ignored $F'$, setting in effect both $S_2$ and $E$ equal to zero. Our slightly weaker magnitudes of synoptic-eddy variance are then consistent with the neglect of $S_2$.

The fact that both we and WS98 produced realistic correlation patterns argues against the importance of the details of the $D$, $E$, $S_1$, and $S_2$ operators. Briefly, if $D + E$ and $S_1 + S_2$ had important structure, WS98's results would not be realistic; and if $E$ and $S_2$ had important structure, our results in Fig. 1 would not be realistic. This then implies that the structures of $D$ and $S_1$ are also unimportant. It need hardly be stated that such broad conclusions are only valid insofar as the simulated and observed synoptic correlation structures are identical in Fig. 1 and in WS98. As stated earlier, this is not the case in Fig. 1 at the eastern ends of the Pacific and Atlantic storm tracks, and there are also significant errors in these regions in WS98's Figs. 6 and 7.

Our simulated amplitudes of intraseasonal (10–90 day) variability, shown in Table 1, are not as realistic as for synoptic variability, partly due to our neglect of intraseasonal tropical heating variations associated with the MJO. Nevertheless, the simulated correlation structures in Fig. 3 are realistic enough to suggest the approximate validity of (5) even on these time scales. Winkler et al. (2001) and Newman et al. (2003) explicitly assumed the dynamics of extratropical intraseasonal variability to be of the form (5), but with an augmented state vector to account also for coherent tropical forcing variations, and then used a Linear Inverse Modeling (LIM) procedure (Penland and Sardeshmukh 1995; Penland and Matrosova 1994) to estimate the $\tilde{M}$ and $S$ operators from observed lag-correlation and fluctuation–dissipation relationships. Remarkably, they found through extensive forecast intercomparisons that the forecast skill of their linear model was competitive with a GCM's skill at week 2 and better than the GCM's skill at week 3 over the Northern Hemisphere. It is hard to imagine how such a linear model would be competitive with comprehensive nonlinear GCMs unless the $T'$ terms could be approximated as in (5) and a significant fraction of the transient diabatic forcing (after explicitly accounting for coherent tropical effects as mentioned above) could be treated as stochastic. Recently, Newman and Sardeshmukh (2008) have demonstrated that the lead–lag correlation structures produced by this linear stochastically driven model are also highly realistic. Similar to the argument given above for the synoptic scales, one can then use this fact and our results in Fig. 3 to argue also for the simplicity of the $D$, $E$, $S_1$, and $S_2$ operators in (5) for intraseasonal scales, with $F'$ now understood to exclude coherent intraseasonal tropical heating variability.

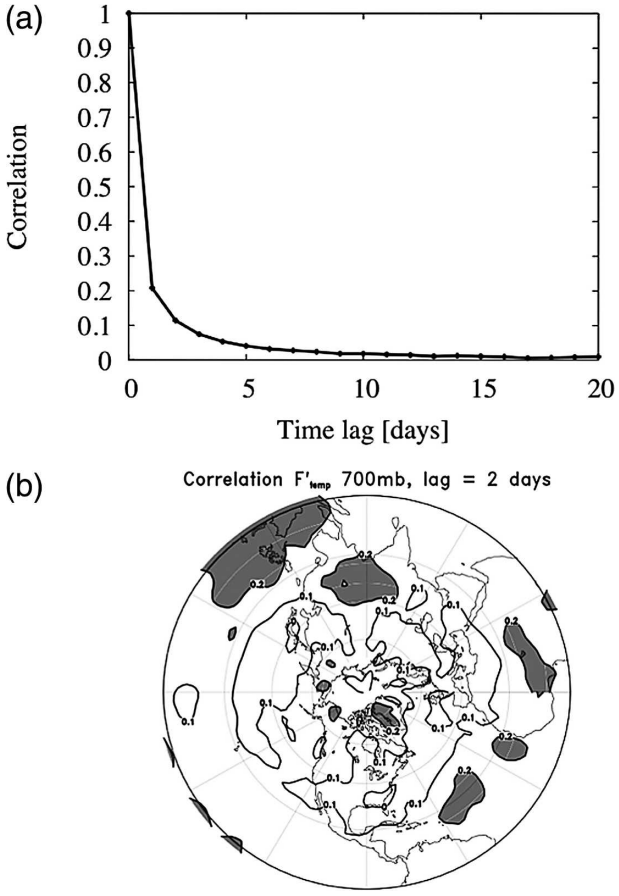


FIG. 13. Time-lag autocorrelation of observed transient diabatic heating at 700 mb. (top) Averaged over all grid points north of 30°N. (bottom) Map of 2-day lag autocorrelations. Values greater than 0.2 are shaded.

Figures 13 and 14 provide direct observational evidence that the autocorrelation of the extratropical transient diabatic forcing $F'$ decays rapidly in both time and space, suggesting that $F'$ may be approximated as a stochastic forcing of synoptic and longer-term circulation variations. For these calculations, $F'$ was estimated for each winter day in 1970–99 as $F - \overline{F}$, where $F$ was estimated as the (sign reversed) initial tendency of the unforced model (1) initialized by the daily averaged 6-hourly observational NCEP–NCAR reanalysis for that day, plus the observed tendency over that 24-h interval. We focus on the statistics of the transient diabatic heating (temperature forcing $F'_T$) at 700 mb, a level of large latent heat release in extratropical weather systems. Figure 13a shows the time-lag autocorrelation function of $F'_T$ averaged over all points

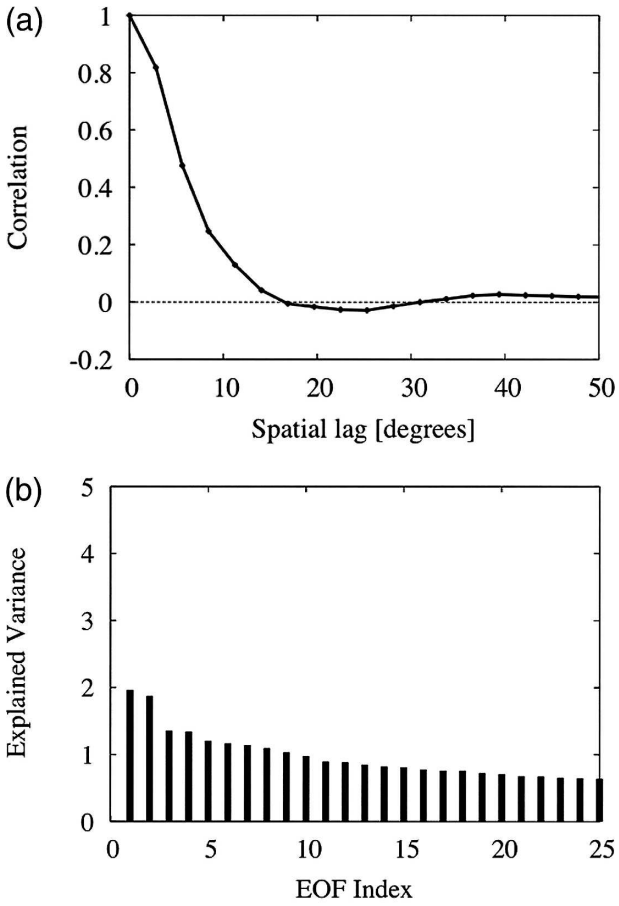


FIG. 14. (top) Average spatial-lag autocorrelation of observed daily diabatic heating fluctuations at 700 mb for all grid points north of 30°N. (bottom) Percentage of the domain-integrated diabatic heating variance explained by the dominant EOFs of the heating fields.

north of 30°N. By day 2 the correlation drops to 0.1. Figure 13b shows the geographical distribution of the 2-day lag autocorrelation of $F'_T$ over the Northern Hemisphere. Consistent with Fig. 13a, the values are close to 0.1 over most of the extratropics.

There is also evidence that a substantial portion of the extratropical $F'$ variability is spatially unstructured. Figure 14a shows the average spatial-lag autocorrelation function of $F'_T$ (700 mb) for all extratropical base points north of 30°N. It shows that on average, the correlation drops to 0.1 at spatial lags of 10°. Displaying the geographical distribution of these lag correlations is complicated by the fact that they do not decay isotropically from each base grid point. To highlight the essentially spatially unstructured character of the $F'_T$ variability, we show instead in Fig. 14b the fractions of variance explained by the EOFs of the extratropical $F'_T$ (700 mb) fields. These fractions are small (less than 2% for the dominant EOF) and decrease very slowly with the EOF index, as expected for the EOFs of spatially unstructured noise.

An autocorrelation decay to 0.1 in Figs. 13 and 14 at lags of 2 days and 10° suggests temporal and spatial autocorrelation scales of about 0.85 days [$\approx -2$ days/ln(0.1)] and 4.3° [$\approx -10°/\ln(0.1)$], respectively, for the $F'_T$ variations. These are close to the smallest resolved scales in our daily averaged observational dataset truncated to T42 spatial resolution, whose effective grid resolution in this context is $360/(2 \times 42) \sim 4.3°$. One may therefore treat these $F'_T$ variations as an effectively white noise forcing of the circulation on the scales of interest in this paper. Even if the forcing is not strictly white but red, one should recall that for a red noise process with correlation scale $\lambda_0$, averages over $2 \times \lambda_0$ are nearly uncorrelated (indeed this fact is often used to estimate the number of degrees of freedom in a red noise series). In our context, this means that variations of $F'_T$ averaged over 1.7 days and 8.6° are effectively uncorrelated and may therefore be treated as a white noise stochastic forcing of circulation variations on longer than these time and space scales. This is clearly an excellent approximation for the intraseasonal and longer-term circulation variations. It is also a reasonable approximation for the synoptic-scale variations, given the evidence in Fig. 1 of significant (anti) correlations at 2-day lags and coherent wavelike structures over much longer distances than 8.6°.

Consistent with the fact that white noise has a flat power spectrum, the observed rapidly decorrelating part of the fluctuating diabatic forcing in both time and space contributes a broadband component to its power spectrum, in both the frequency and wavenumber domains, rather than just a "high-frequency" component. This broadband character makes the stochastic component of the transient forcing an efficient facilitator of multiscale interactions in the climate system, across both space and time scales.

## 6. Discussion and concluding remarks

The deficiencies of our constant-forcing simulation indicate a substantial role for transient diabatic forcing in the dynamics of atmospheric circulation variability and the mean climate. In particular, the reduced magnitudes but realistic structures of our simulated variability suggest a role for the stochastic components of the transient forcing. Given the relatively low resolution of our model and its simple representations of mechanical and thermal damping, a precise quantification

of this role is difficult, but the general conclusion is clear. An obvious next step would be to repeat such constant-forcing simulations with higher-resolution dry adiabatic GCMs with more sophisticated treatments of mechanical and thermal damping. This is a topic of current research.

What particular aspects of the variable forcing, in what geographical regions, and on what time scales, are relatively more important? We have not addressed this issue, although Table 1 is certainly consistent with numerous studies showing the impact of MJO heating on intraseasonal variability and of ENSO on interannual variability. A more quantitative assessment could be made by adding various components of the transient forcing to the constant forcing in our nonlinear dry adiabatic GCM and assessing their impacts on the simulated variability and the mean climate. In pursuing these extensions, one would need to be more mindful of the forcing-circulation decoupling issue, especially in diagnosing the effects of latent heat release in extratropical weather systems, than in our constant-forcing study here. Nonetheless, we believe that the effects of the stochastic components of the transient forcing, as well as of coherent tropical forcing, on the extratropical circulation could be diagnosed fruitfully in such extended studies. We note that most previous studies of such effects have been performed with linear models, not nonlinear models such as ours that simulate transient eddies and allow for nonlinear transient-eddy/mean-flow interactions.

Our neglect of coherent latent heat release feedbacks in extratropical weather systems leads to notable deficiencies at the ends of the Pacific and Atlantic storm tracks in Fig. 1, and also to a much smaller 700-mb poleward heat flux at 45°N in Fig. 8. Our constant forcing simulation is useful in suggesting these net impacts. However, it is not clear if further diagnosis is justified by treating the latent heat release as an external forcing. Allowing for some state dependence, at a minimum of the linear form (5), may prove essential for the clarification of such extratropical diabatic effects.

Nonetheless, we have provided both direct and indirect evidence that extratropical transient diabatic effects have a stochastic component that may be treated as a stochastic forcing. A stochastic component of tropical diabatic forcing is also suggested by the study of Ricciardulli and Sardeshmukh (2002), who found even shorter temporal (~6 h) and spatial (~150 km) correlation scales associated with tropical deep convective variability.

In summary, our results suggest a substantial role for both coherent and stochastic diabatic forcing variability in the dynamics of atmospheric circulation variability and the mean climate. These effects span across time scales. The effect on the mean climate occurs through the effect of the transient forcing on the mean transient-eddy momentum and heat fluxes. The transient forcing not only directly influences the circulation variability on each time scale but also facilitates interactions across scales through its influence on the adiabatic fluxes. The broadband stochastic component of the diabatic forcing is an efficient facilitator in this regard. Improving the representation of both coherent and stochastic diabatic forcing thus has implications for improving simulations and predictions on all time scales in the climate system.

*Acknowledgments.* We thank the Hamburg PUMA modeling group for help with the PUMA model, and M. Newman for help with both the PUMA model and the chi-corrected NCEP reanalyses. Discussions with our colleagues at the Climate Diagnostics Center, especially C. Penland, are also gratefully acknowledged. This research was partly supported by funding from the Office of Naval Research and NOAA's Office of Global Programs.

## REFERENCES

Anderson, J. L., and Coauthors, 2004: The new GFDL global atmosphere and land model AM2–LM2: Evaluation with prescribed SST simulations. *J. Climate,* **17,** 4641–4673.

Asselin, R., 1972: Frequency filter for time integrations. *Mon. Wea. Rev.,* **100,** 487–490.

Compo, G. P., and P. D. Sardeshmukh, 2004: Storm-track predictability on seasonal and decadal scales. *J. Climate,* **17,** 3701–3720.

——, ——, and C. Penland, 2001: Changes of subseasonal variability associated with El Niño. *J. Climate,* **14,** 3356–3374.

Delsole, T., 2004: Stochastic models of quasigeostrophic turbulence. *Surv. Geophys.,* **25,** 107–149.

Duchon, C. E., 1979: Lanczos filtering in one and two dimensions. *J. Appl. Meteor.,* **18,** 1016–1022.

Farrell, B. F., and P. J. Ioannou, 1995: Stochastic dynamics of the midlatitude atmospheric jet. *J. Atmos. Sci.,* **52,** 1642–1656.

Fraedrich, K., H. Jansen, E. Kirk, U. Luksch, and F. Lunkeit, 2005a: The Planet Simulator: Toward a user friendly mode. *Meteor. Z.,* **14,** 299–304.

——, ——, ——, and F. Lunkeit, 2005b: The Planet Simulator: Green planet and desert world. *Meteor. Z.,* **14,** 305–314.

——, E. Kirk, U. Luksch, and F. Lunkeit, 2005c: The portable university model of the atmosphere (PUMA): Storm track dynamics and low-frequency variability. *Meteor. Z.,* **14,** 735–745.

Gates, W. L., and Coauthors, 1999: An overview of the results of the Atmospheric Model Intercomparison Project (AMIP I). *Bull. Amer. Meteor. Soc.,* **80,** 29–55.

Hall, N. M. J., 2000: A simple GCM based on dry dynamics and constant forcing. *J. Atmos. Sci.,* **57,** 1557–1572.

——, and P. D. Sardeshmukh, 1998: Is the time-mean Northern Hemisphere flow baroclinically unstable? *J. Atmos. Sci.,* **55,** 41–56.

Hoskins, B. J., and A. J. Simmons, 1975: A multi-layer spectral model and semi-implicit method. *Quart. J. Roy. Meteor. Soc.,* **101,** 637–655.

Hurrell, J. W., J. J. Hack, A. S. Phillips, J. Caron, and J. Yin, 2006: The dynamical simulation of the Community Atmosphere Model Version 3 (CAM3). *J. Climate,* **19,** 2162–2183.

Lin, H., and J. Derome, 1996: Changes in predictability associated with the PNA pattern. *Tellus,* **48A,** 553–571.

Marshall, J., and F. Molteni, 1993: Toward a dynamical understanding of planetary-scale flow regimes. *J. Atmos. Sci.,* **50,** 1792–1818.

Newman, M., and P. D. Sardeshmukh, 2008: Tropical and stratospheric influences on extratropical short-term climate variability. *J. Climate,* in press.

——, ——, C. R. Winkler, and J. S. Whitaker, 2003: A study of subseasonal predictability. *Mon. Wea. Rev.,* **131,** 1715–1732.

Penland, C., and L. Matrosova, 1994: A balance condition for stochastic numerical models with application to the El Niño–Southern Oscillation. *J. Climate,* **7,** 1352–1372.

——, and P. D. Sardeshmukh, 1995: The optimal growth of tropical sea surface temperature anomalies. *J. Climate,* **8,** 1999–2024.

Ricciardulli, L., and P. D. Sardeshmukh, 2002: Local time and space scales of organized tropical deep convection. *J. Climate,* **15,** 2775–2790.

Roads, J. O., 1987: Predictability in the extended range. *J. Atmos. Sci.,* **44,** 3495–3527.

Robinson, D. P., and R. X. Black, 2005: The statistics and structure of subseasonal midlatitude variability in NASA GSFC GCMs. *J. Climate,* **18,** 3294–3316.

Sardeshmukh, P. D., 1993: The baroclinic $\chi$ problem and its application to the diagnosis of atmospheric heating rates. *J. Atmos. Sci.,* **50,** 1099–1112.

——, M. Newman, and C. R. Winkler, 1999: Dynamically consistent estimates of diabatic heating. *Proc. 24th Annual Climate Diagnostics and Prediction Workshop,* Tucson, AZ, NOAA, 172–175.

——, G. P. Compo, and C. Penland, 2000: Changes of probability associated with El Niño. *J. Climate,* **13,** 4268–4286.

Wallace, J. M., and D. S. Gutzler, 1981: Teleconnections in the geopotential height field during the Northern Hemisphere winter. *Mon. Wea. Rev.,* **109,** 784–812.

Whitaker, J. S., and P. D. Sardeshmukh, 1998: A linear theory of extratropical synoptic eddy statistics. *J. Atmos. Sci.,* **55,** 237–258.

Winkler, C. R., M. Newman, and P. D. Sardeshmukh, 2001: A linear model of wintertime low-frequency variability. Part I: Formulation and forecast skill. *J. Climate,* **14,** 4474–4494.